



# Two-Dimensional Rotation of Chaotic Attractors: Demonstrative Examples and FPGA Realization

W. S. Sayed<sup>1</sup> · A. G. Radwan<sup>1,2</sup>  · M. Elnawawy<sup>3</sup> · H. Orabi<sup>3</sup> · A. Sagahyoon<sup>3</sup> · F. Aloul<sup>3</sup> · A. S. Elwakil<sup>2,4,5</sup> · H. A. Fahmy<sup>6</sup> · A. El-Sedeek<sup>1</sup>

Received: 5 December 2018 / Revised: 16 March 2019 / Accepted: 19 March 2019  
© Springer Science+Business Media, LLC, part of Springer Nature 2019

## Abstract

In this work, we demonstrate the possibility of performing two-dimensional rotation on a chaotic system. This enables the rotation of its attractor in space without changing its chaotic dynamics. In particular, the rotated system preserves the same eigenvalues at all equilibrium points and its largest Lyapunov exponent remains unchanged. Two chaotic systems, one of which is the classical Lorenz system, are used to illustrate and validate the rotation operation using numerical simulations and further experimentally using a digital FPGA platform.

**Keywords** Chaotic oscillators · Digital chaos generation · FPGA · Two-dimensional rotation

## 1 Introduction and Background

Chaos theory studies aperiodic sequences, which are unpredictable on the long term but are generated from deterministic relations [1]. Chaos is observed in many biological, chemical [22], electronic [20] and financial systems [9] and has important applications, particularly in chaos-based communications and cryptography [12–14,19]. Several encryption schemes are now based on continuous-time chaotic systems [24] and their modified fractional-order versions [11,25].

Meanwhile, two-dimensional vector rotation is a standard and well-known operation that can be performed on various trajectories. In particular, a system of differential equations  $\dot{\underline{x}} = \underline{f}(\underline{x})$  in the original coordinate system  $\underline{x}$  can be transformed to the rotated coordinate system  $\underline{u}$  using a rotation matrix  $R$ . Thus,  $\underline{u} = R\underline{x}$ , and hence  $\underline{x} = R^{-1}\underline{u}$ . The rotated system of differential equations is given by  $\dot{\underline{u}} = R\dot{\underline{x}} = R\underline{f}(\underline{x}) = R\underline{f}(R^{-1}\underline{u})$ .

---

Extended author information available on the last page of the article

In a space of two dimensions  $x$  and  $y$ , the rotated axes  $u$  and  $v$  can be given by:

$$\begin{bmatrix} u \\ v \end{bmatrix} = R \begin{bmatrix} x \\ y \end{bmatrix} = \begin{bmatrix} \cos \theta & \sin \theta \\ -\sin \theta & \cos \theta \end{bmatrix} \begin{bmatrix} x \\ y \end{bmatrix}, \quad (1)$$

where  $\theta$  is the angle of rotation in the  $x - y$  plane. This can also be considered as the rotation angle about the  $z$ -axis in a 3D space or equivalently

$$\begin{bmatrix} u \\ v \\ w \end{bmatrix} = \begin{bmatrix} \cos \theta & \sin \theta & 0 \\ -\sin \theta & \cos \theta & 0 \\ 0 & 0 & 1 \end{bmatrix} \begin{bmatrix} x \\ y \\ z \end{bmatrix}, \quad (2)$$

which means that the coordinate  $z$  does not change, i.e.,  $w = z$ . Consequently, the governing differential equations of the rotated variables  $u$  and  $v$  in terms of  $x$  and  $y$  are given by:

$$\begin{aligned} \dot{u} &= \cos \theta \dot{x} + \sin \theta \dot{y}, \\ \dot{v} &= -\sin \theta \dot{x} + \cos \theta \dot{y}. \end{aligned} \quad (3)$$

In this work, we seek to illustrate the possibility of rotating chaotic attractors and show that the dynamics do not change as a result of this rotation because the eigenvalues at all equilibrium points remain unchanged. We first consider the famous Lorenz system [15]

$$\begin{aligned} \dot{x} &= a(y - x), \\ \dot{y} &= (b - z)x - y, \\ \dot{z} &= xy - cz, \end{aligned} \quad (4)$$

where  $(a, b, c)$  are parameters. In particular, we show that its butterfly attractor can be rotated in the  $x - y$  plane with a rotation angle  $\theta \in (-\pi, \pi]$ . We also show that dynamic rotation of the attractor, whereby the rotation angle changes with time rather than being a constant, is possible. This may be particularly important for security applications based on chaos since the information can be encoded dynamically in the rotating angle with no fear of changing the chaotic dynamics of the system.

In a second example, we demonstrate the rotation in the  $x - y$  plane of the chaotic attractor from the canonical switching-type system proposed in [6] and given by

$$\begin{aligned} \dot{x} &= y, \\ \dot{y} &= z, \\ \dot{z} &= -a(x + y + z - \operatorname{sgn}(x)), \end{aligned} \quad (5)$$

where  $a$  is a parameter and  $\operatorname{sgn}(x)$  is the signum function defined as

$$\operatorname{sgn}(x) = \begin{cases} -1, & x < 0, \\ 0 & x = 0, \\ 1, & x > 0. \end{cases} \quad (6)$$

Finally, we verify in hardware the two-dimensional rotation using an FPGA to synthesize and test the systems, which is much easier than using analog circuit implementations. That is why efficient realizations of many chaotic systems have recently been presented on digital platforms, including DSPs and FPGAs [5,17,23,26,27]. In addition, Lorenz system has inspired many researchers to develop modified versions of this attractor and their hardware realizations [2,7,8,16,18]. However, we note that despite the unchanged chaotic dynamics, the original  $z(t)$  signal diverges from  $w(t)$  in the rotated system due to the limited step size used in the discretized versions of the chaotic equations implemented on the FPGA.

## 2 Two-Dimensional Rotation About the z-Axis

### 2.1 Lorenz System

The system (4) in the rotated coordinates  $u, v$  and the renamed coordinate  $w$  is given by:

$$\begin{aligned}\dot{u} &= \cos \theta (a((-\sin \theta u + \cos \theta v) - (\cos \theta u + \sin \theta v))) \\ &\quad - \sin \theta ((b - w)(\cos \theta u + \sin \theta v) - (\cos \theta v - \sin \theta u)), \\ \dot{v} &= \sin \theta (a((-\sin \theta u + \cos \theta v) - (\cos \theta u + \sin \theta v))) \\ &\quad + \cos \theta ((b - w)(\cos \theta u + \sin \theta v) - (\cos \theta v - \sin \theta u)), \\ \dot{w} &= (\cos \theta u + \sin \theta v)(-\sin \theta u + \cos \theta v) - cw.\end{aligned}\quad (7)$$

This system of equations can be simplified through defining

$$\begin{aligned}T_1 &= \cos \theta u + \sin \theta v, \\ T_2 &= -\sin \theta u + \cos \theta v\end{aligned}\quad (8)$$

resulting in the rotated Lorenz system described by

$$\begin{aligned}\dot{u} &= a \cos \theta (T_2 - T_1) - \sin \theta ((b - w)T_1 - T_2), \\ \dot{v} &= a \sin \theta (T_2 - T_1) + \cos \theta ((b - w)T_1 - T_2), \\ \dot{w} &= T_1 T_2 - cw.\end{aligned}\quad (9)$$

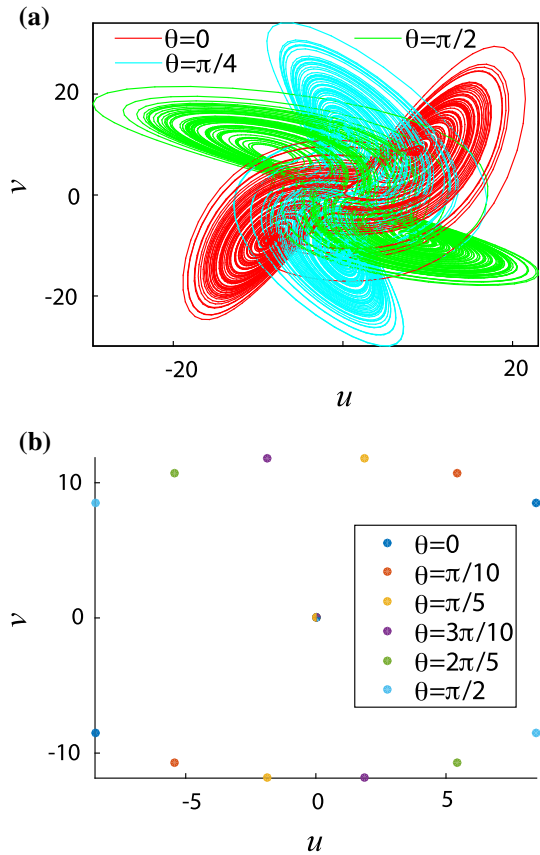
In order to realize this system later on an FPGA, we consider its Euler discretized form as

$$\begin{aligned}u_{i+1} &= u_i + h (a \cos \theta (T_2 - T_1) - \sin \theta ((b - w_i)T_1 - T_2)), \\ v_{i+1} &= v_i + h (a \sin \theta (T_2 - T_1) + \cos \theta ((b - w_i)T_1 - T_2)), \\ w_{i+1} &= w_i + h (T_1 T_2 - cw_i),\end{aligned}\quad (10)$$

with  $T_1$  and  $T_2$  evaluated at  $u_i$  and  $v_i$ , respectively.  $h$  is a constant step which is fixed throughout this work to  $h = 0.01$ .

Figure 1a presents the numerical simulation results of the rotated Lorenz attractor for different phase angles with  $a = 10$ ,  $b = 28$  and  $c = 8/3$  projected

**Fig. 1** Rotated Lorenz chaotic attractor **a** projection in the  $u - v$  plane and **b** rotation of the equilibrium points

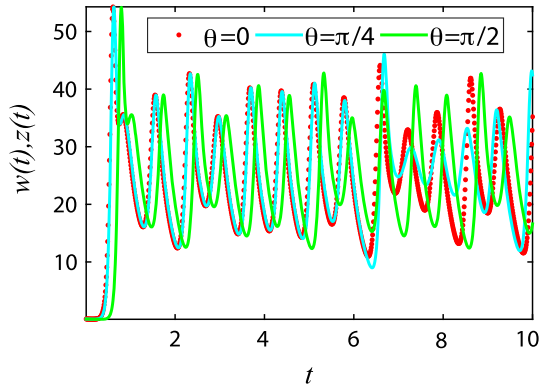


in the  $u - v$  plane. The reference trajectory at  $\theta = 0$  is plotted in red, and the rotating trajectories at  $\theta = \pi/4$  and  $\theta = \pi/2$  are also plotted. The new attractors are rotated versions in the anticlockwise direction as a result of rotating the equilibrium points in the  $u - v$  plane, as shown in Fig. 1b. The equilibrium points of the system at the given parameter values are, respectively,  $(0, 0, 0)$  and  $(\pm 8.48528 (\cos \theta - \sin \theta), \pm 8.48528 (\cos \theta + \sin \theta), 27)$ . The corresponding Jacobian is given by

$$J = \begin{bmatrix} \left( \frac{w}{2} - 19 \right) \sin 2\theta - \frac{9 \cos 2\theta}{2} - \frac{11}{2} & (38 - w) \cos^2 \theta - \frac{9 \sin 2\theta}{2} + w - 28 & T_1 \sin \theta \\ (38 - w) (\cos \theta)^2 - \frac{9 \sin 2\theta}{2} - 10 - \left( \frac{w}{2} - 19 \right) \sin 2\theta + \frac{9 \cos 2\theta}{2} - \frac{11}{2} & -T_1 \cos \theta \\ v \cos 2\theta - u \sin 2\theta & u \cos 2\theta + v \sin 2\theta & -\frac{8}{3} \end{bmatrix} \quad (11)$$

The equilibrium points and the Jacobian matrix of the rotated system differ from the original system. Yet, the characteristic polynomial evaluated at the equilibrium points results in eigenvalues that are identical to those of the original system as follows. The characteristic polynomial is given by:

**Fig. 2** Deviation of  $w(t)$  from  $z(t)$  at three different values of  $\theta$ . Note that  $w(t) = z(t)$  at  $\theta = 0$



$$\lambda^3 - \text{tr}(J)\lambda^2 + (M_{11} + M_{22} + M_{33})\lambda - |J| = 0, \tag{12}$$

where  $\text{tr}(J)$  is the trace of the Jacobian matrix,  $|J|$  is its determinant and  $M_{ij}$  is the minor determinant of the matrix  $J$  by removing the  $i$ th row and  $j$ th column. The coefficients of the characteristic polynomial are obtained as follows:

- $\text{tr}(J) = -\frac{11}{2} - \frac{11}{2} - \frac{8}{3} = -\frac{41}{3}$ .
- $M_{11} = 0.5u^2 \cos 2\theta + 0.5u^2 \cos^2 2\theta - 0.5v^2 \cos^2 2\theta + 0.5v^2 + 0.5uv \sin 2\theta + 0.5uv \sin 4\theta + \frac{4}{3}w \sin 2\theta - 12 \cos 2\theta - \frac{152}{3} \sin 2\theta + \frac{44}{3}$ .
- $M_{22} = -0.5u^2 \cos^2 2\theta + 0.5u^2 - 0.5v^2 \cos 2\theta + 0.5v^2 \cos^2 2\theta + 0.5uv \sin 2\theta - 0.5uv \sin 4\theta - \frac{4}{3}w \sin 2\theta + 12 \cos 2\theta + \frac{152}{3} \sin 2\theta + \frac{44}{3}$ .
- $M_{33} = 10w - 270$ .
- and hence  $M_{11} + M_{22} + M_{33} = 0.5(1 + \cos 2\theta)u^2 + 0.5(1 - \cos 2\theta)v^2 + uv \sin 2\theta + 10w - \frac{722}{3}$ .
- $|J| = 5(\sin 2\theta - \cos 2\theta - 1)u^2 + 5(\cos 2\theta - \sin 2\theta - 1)v^2 - 10(\cos 2\theta + \sin 2\theta)uv - \frac{80}{3}w + 720$ .

Consequently,  $\text{tr}(J)$  is always independent of  $\theta$ . At the equilibrium point  $(0, 0, 0)$ ,  $M_{11} + M_{22} + M_{33} = -\frac{722}{3}$  and  $|J| = 720$ . Hence, the characteristic polynomial evaluated at the equilibrium point  $(0, 0, 0)$  and the resulting eigenvalues are independent of  $\theta$  and identical to those of the original system. This result was similarly validated for the other two equilibrium points, where  $M_{11} + M_{22} + M_{33} = \frac{304}{3}$  and  $|J| = -1440$ .

In conclusion, a symbolic derivation of the characteristic polynomials followed by the substitution by these different equilibrium points results in eigenvalues that are identical to those of the original system. Hence, the original and rotating systems have the same eigenvalues, respectively, at the three equilibrium points. Thus, the rotation does not change the chaotic dynamics. However, the rotation results in a  $w(t)$  time series that differs from the original  $z(t)$  time series due to the sensitivity of the chaotic system to initial conditions and the finite discretization step  $h$ . This is clearly shown in Fig. 2.

Bifurcation diagrams of the three state variables against  $\theta$  are shown in Fig. 3 after discarding the first 2000 points in each simulation. The figures show that the chaotic behavior is preserved independent of  $\theta$  over the whole range  $\theta \in (-\pi, \pi]$  with

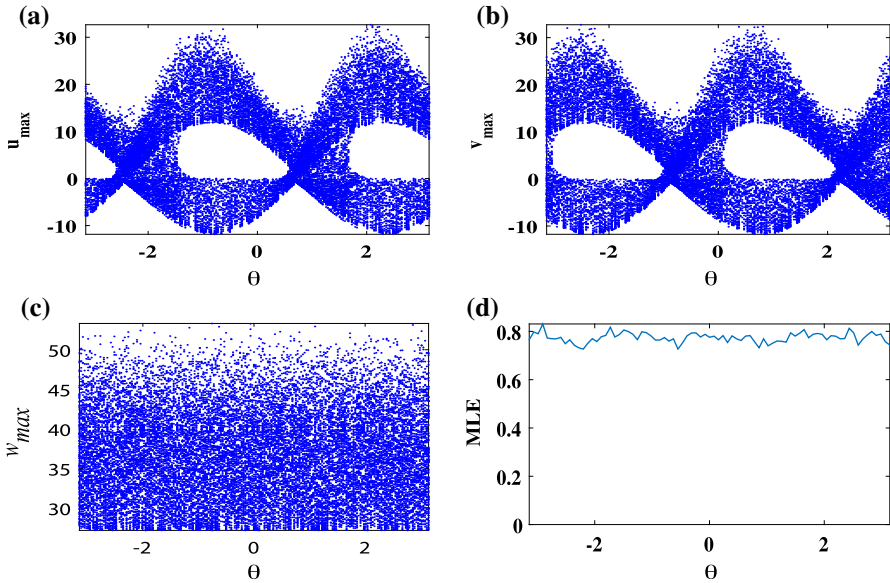


**Fig. 3** Bifurcation diagrams of **a**  $u$ , **b**  $v$  and **c**  $w$  and **d** MLE versus  $\theta$

no islands of stability, as expected. A finite positive maximum Lyapunov exponent indicates chaotic behavior and is a target for maximization against the parameters [4]. The calculated maximum Lyapunov exponent of the system was found to remain positive, independent of  $\theta$ , fluctuating around the value of 0.8 as shown in Fig. 3d. In conclusion, it is evident that the rotation angle does not change the chaotic dynamics of the system or force it into any possible periodic mode of operation.

The effect of rotation on the eigenvectors of the Jacobian matrix is also studied, where their values at the third equilibrium point are given in Table 1. In addition, the eigenvectors inclination (EVI) is plotted against the rotation angle  $\theta$ . EVI is the angle between the vector at  $\theta = 0$  and that at a given value of  $\theta$ . In a real inner product space, the angle  $\phi$  between two vectors  $x$  and  $y$  is defined by  $\cos \phi = \frac{\langle x, y \rangle}{\|x\| \|y\|}$ . In a complex vector space, taking the real part of this cosine defines the Euclidean angle as  $\cos \phi_E = \frac{\Re\{\langle x, y \rangle\}}{\|x\| \|y\|}$ . Figure 4 shows that EVI ( $\phi_E$ ) follows a pattern similar to that of the rotating system itself where EVI is plotted at the third equilibrium point, as an example. The same holds for the other equilibrium points.

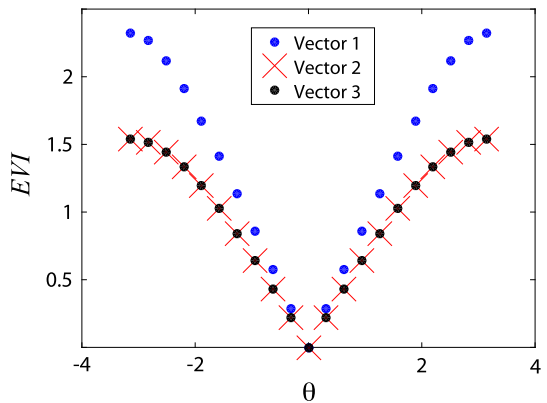
## 2.2 Dynamic Rotation

To demonstrate the possibility of encoding information into the phase rotation angle, we consider  $\theta$  as a dynamic signal with two different cases, as shown in Table 2. Switching the sign of a parameter such that it varies dynamically with time was used in [8] to generate the four-wing Lorenz attractor. This switch in sign can be considered as a phase rotation of  $\pi$ . By introducing this dynamic rotation, it is possible to increase the number of parameters that can be used to encode information for example by using

**Table 1** Eigenvalues and eigenvectors of Lorenz and rotated Lorenz systems at the third equilibrium point

Lorenz	Rotated Lorenz
$\lambda_1 = -13.85,$	$\lambda_1 = -13.85,$
$\lambda_{2,3} = 0.09396 \pm 10.19 i$	$\lambda_{2,3} = 0.09396 \pm 10.19 i$
$V_1 = \begin{bmatrix} -2.146 \\ 0.827 \\ 1 \end{bmatrix}$	$V_1 = \begin{bmatrix} -2.146 \cos \theta - 0.827 \sin \theta \\ 0.827 \cos \theta - 2.146 \sin \theta \\ 1 \end{bmatrix}$
$V_{2,3} = \begin{bmatrix} 0.37 \pm 0.4102 i \\ -0.04467 \pm 0.7912 i \\ 1 \end{bmatrix}$	$V_{2,3} = \begin{bmatrix} \cos \theta (0.37 \pm 0.4102 i) + \sin \theta (0.04467 \mp 0.7912 i) \\ \cos \theta (-0.04467 \pm 0.7912 i) + \sin \theta (0.37 \mp 0.4102 i) \\ 1 \end{bmatrix}$

**Fig. 4** Eigenvectors inclination (EVI) against the rotation angle  $\theta$  at the third equilibrium point



the amplitude  $A$  and/or period  $T$  (see Table 2). Since no periodic windows or change in the Lyapunov exponents spectrum is observed due to rotation, the information encoding within the rotation angle parameters is an attractive option. Projections of the dynamically rotated Lorenz attractor are shown within Table 2 for the case of a sinusoidal function as well as for a staircase function.

### 2.3 Switching-Type System

The system (5) in the rotated coordinates  $(u, v, w)$  in Euler form can be written as

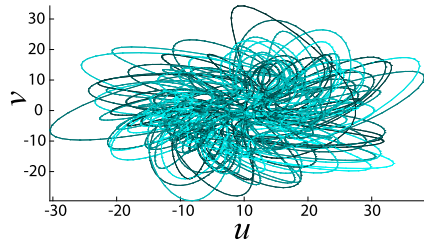
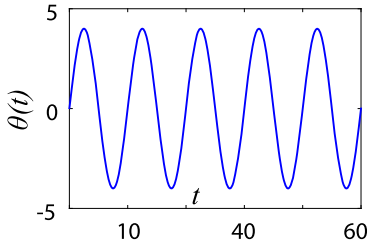
$$\begin{aligned}
 u_{i+1} &= u_i + h (T_3 \cos \theta + \sin \theta w), \\
 v_{i+1} &= v_i + h (-T_3 \sin \theta + \cos \theta w), \\
 w_{i+1} &= w_i - ha (T_3 + T_4 + w - \text{sgn}(T_4)),
 \end{aligned}
 \tag{13}$$

where

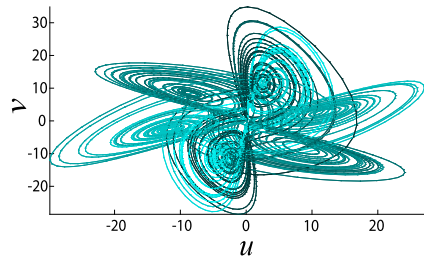
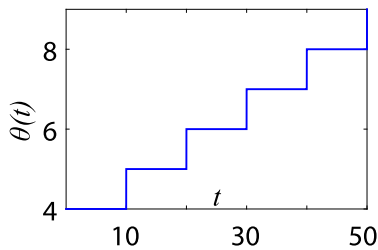
$$\begin{aligned}
 T_3 &= \sin \theta u + \cos \theta v, \\
 T_4 &= \cos \theta u - \sin \theta v
 \end{aligned}
 \tag{14}$$

**Table 2** Possible dynamic signals with amplitude  $A$  and period  $T$  used for dynamic rotation ( $A = 10, T = 50$ )

$$\theta = 10 \sin\left(\frac{2\pi t}{50}\right)$$



$$\theta = 10 + \lfloor \frac{t}{50} \rfloor$$



and  $sgn(T_4)$  is the signum function. Figure 5a shows the numerical simulation results of the rotated attractor with  $a = 0.8$  at three different angles. The equilibrium points  $(\cos \theta sgn(T_4), -\sin \theta sgn(T_4), 0)$  have a corresponding Jacobian given by (15)

$$J = \begin{bmatrix} \cos \theta \sin \theta & \cos^2 \theta & \sin \theta \\ -\sin^2 \theta & -\cos \theta \sin \theta & \cos \theta \\ -0.8 (\cos \theta + \sin \theta) & -0.8 (\cos \theta - \sin \theta) & -0.8 \\ +1.6 \cos \theta \delta(T_4) & -1.6 \sin \theta \delta(T_4) & \end{bmatrix} \quad (15)$$

for  $a = 0.8$ .

We again verify that the un-rotated and rotated systems have the same eigenvalues at all equilibrium points. Hence, the rotation process does not change the chaotic dynamics. However, as mentioned earlier for the Lorenz system,  $w(t)$  deviates from  $z(t)$  due to the fixed value of  $h$  albeit with no periodic windows at any value of  $\theta$  as shown in Fig. 5b.

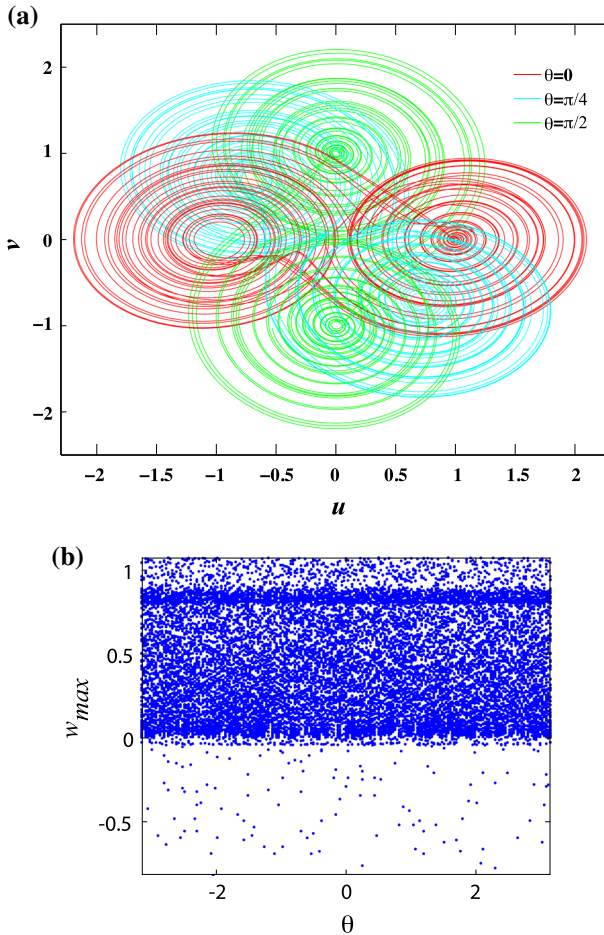


**Fig. 5** Rotated switching-type chaotic attractor **a** projection in the  $u - v$  plane and **b** bifurcation diagram of  $w$  versus  $\theta$

### 3 FPGA Realization

Advent in technology has led to the development of highly dense and reliable FPGA platforms that are currently being used in applications such as image and packet processing, accelerating the execution of machine learning algorithms, and recently in the design of chaotic systems [3,21]. The systems of Eqs. (10) and (13) were implemented using the experimental setup shown in Fig. 6. The platform used is the DE2-115 development board equipped with Intel @Cyclone IV FPGA EP4CE115F29C7 device. These devices are suitable for low-cost, low-power and small form factor applications. Cyclone IV has 114,480 logic elements, 300  $9 \times 9$  multipliers, 266  $18 \times 18$  multipliers, 3888 K of embedded memory, 4 general-purpose PLLs, 8 user I/O Banks and 528 maximum user I/O. For the work discussed here, a data conversion card with two DAC5762 14-bit 275 MSPS is interfaced with the FPGA platform as shown in Fig. 6.

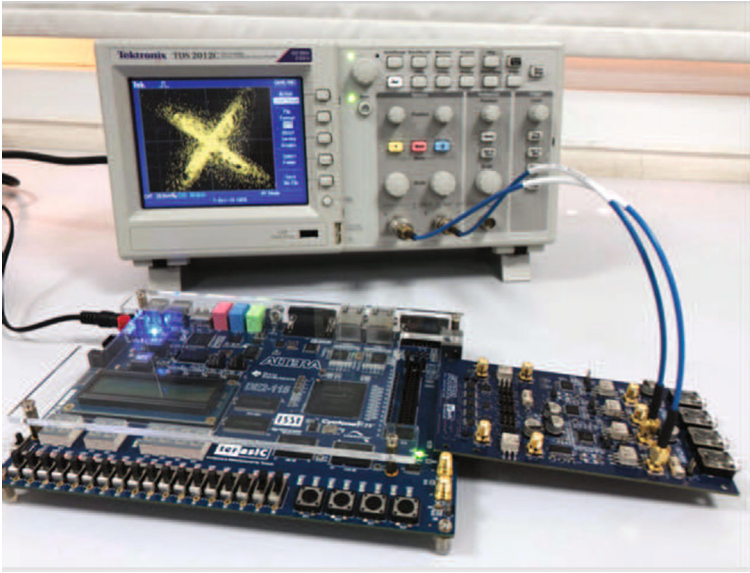


Fig. 6 Experimental FPGA setup and results of the dynamic angle rotation shown on the oscilloscope

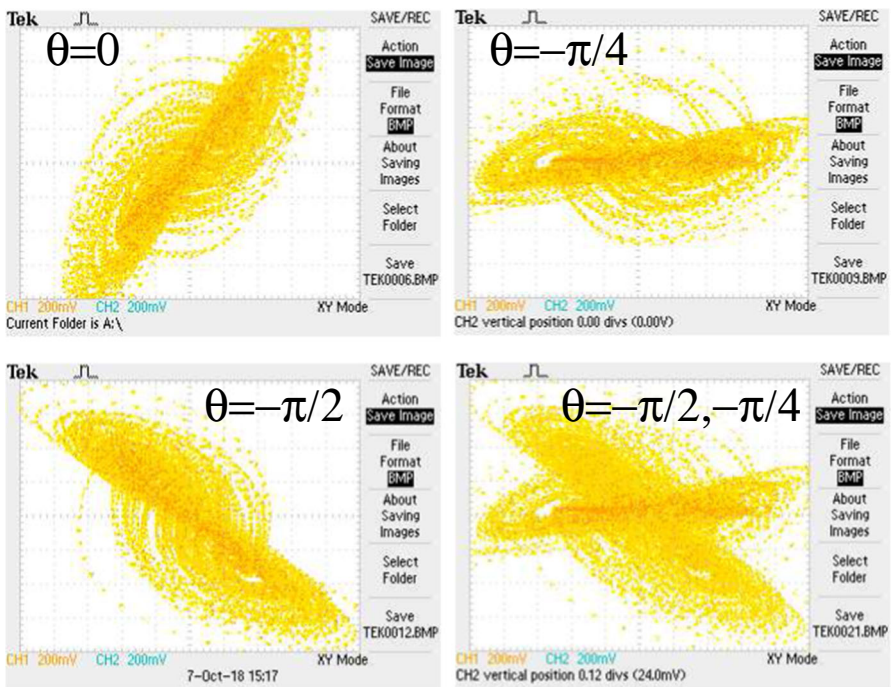
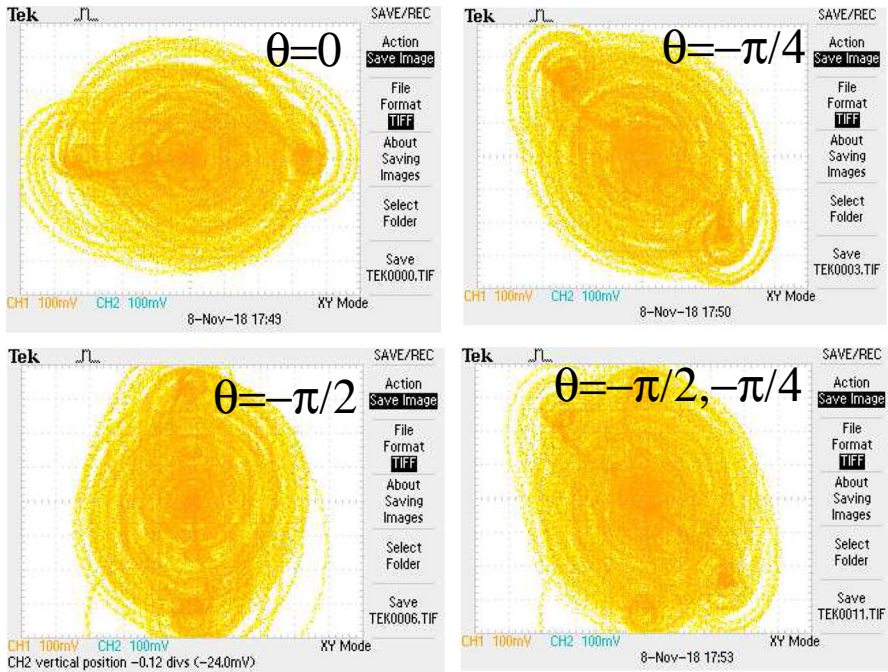


Fig. 7 Experimental results showing the  $u-v$  projection of the chaotic Lorenz attractor rotated by  $-\pi/4$ ,  $-\pi/2$  and dynamic switching between these two angles of rotation



**Fig. 8** Experimental FPGA results of the switching system showing the  $u - v$  projection of the chaotic attractor rotated by  $-\pi/4$ ,  $-\pi/2$  and dynamic switching between these two angles

Initially, the MATLAB/Simulink HDL coder was used to generate the RTL code of the chaotic system. However, the generated code was far from optimal [3], and hence we opted to build the system using Verilog and the Quartus environment from Intel [10]. The code was verified by performing functional and timing simulation using ModelSim [10] and was also verified after prototyping using a standard logic analyzer.

At the heart of the code are three core modules responsible for the generation of the output state variables  $u(t)$ ,  $v(t)$  and  $w(t)$  for a specific rotation angle using 32-bit fixed point arithmetic. For testing purposes, the implemented rotation angles were  $0$ ,  $\pm\pi/4$  and  $\pm\pi/2$ . Arithmetic operators in each module are implemented using IP cores from Intel. The DACs output is displayed on oscilloscope as shown in Fig. 6. A data conversion card with a 14-bit resolution two-channel digital-to-analog (D/A) converter was interfaced and used with the board as shown in Fig. 6 to observe the output on the oscilloscope. Finally, a phase-locked loop (PLL) was used to generate the system clock of 15 MHz for the rotated Lorenz system and 24 MHz for the switching system, ensuring that its phase matches with that of the internal DE2-115 board's oscillator. Multiplication operations were converted to shift and add operations to save resources where possible.

Experimental results of the rotated Lorenz system are shown in Fig. 7 which shows the observed attractors in the  $u - v$  plane, respectively, rotated by  $-\pi/4$  and  $-\pi/2$  compared to the original non-rotated version. Further, dynamic switching between these two rotation angles using a simple binary switching function is also shown. Figure 8 represents the experimental results of the switching-type system rotated

**Table 3** Summary of used FPGA resources

Resources	Rotated Lorenz system	Rotated switching-type system
Logic elements	3543/114480 (3%)	1873/114480 (2%)
Combinational functions	3490	1869
Registers	736	721
Embedded multiplier (9-bit)	48/532 (9%)	0/532
Pins	41/529 (8%)	38/529 (7%)
PLL	1	1
Frequency	15 MHz	24 MHz

**Table 4** MAE for the different rotations

Degree	MAE <sub>u</sub>	MAE <sub>v</sub>	MAE <sub>w</sub>
0	0.0717	0.0695	0.0624
$\pi/4$	0.0617	0.0571	0.0540
$\pi/2$	0.0407	0.0435	0.0366

also in the  $u - v$  plane by  $-\pi/4$  and  $-\pi/2$ . The hardware resources utilized in the implementations of the two systems are summarized in Table 3 showing efficient hardware utilization.

To assess the validity of our FPGA realization, we have used a logic analyzer to capture the values of  $u$ ,  $v$  and  $w$  from the FPGA for the three angles  $0$ ,  $\pi/4$  and  $\pi/2$ . The obtained values are then fed into MATLAB such that they can be compared with the ideal simulation values. Table 4 lists the mean absolute errors (MAEs) between the simulation values and the values obtained from the FPGA realization for the first 5000 iterations.

## 4 Conclusions

We have demonstrated theoretically and experimentally the possible 2D rotation of chaotic attractors applied to two different chaotic system prototypes. The rotation operation does not change the eigenvalues at the respective equilibrium points of the chaotic system, and hence it does not change the global dynamical behavior of the system. This is an attractive feature which can be exploited in chaos-based encryption applications and needs to be further investigated in addition to exploring the possibility of 3D rotation. FPGA implementations of two rotated chaotic systems show reasonable use of resources, indicating that the technique is not hardware intensive.

## Compliance with Ethical Standards

**Conflict of Interest** The authors declare that they have no conflict of interest.

## References

1. K.T. Alligood, T.D. Sauer, J.A. Yorke, *Chaos: An Introduction to Dynamical Systems* (Springer, Berlin, 1996)
2. M.L. Barakat, A.S. Mansingka, A.G. Radwan, K.N. Salama, Generalized hardware post-processing technique for chaos-based pseudorandom number generators. *ETRI J.* **35**(3), 448–458 (2013)
3. T. Bonny, A.S. Elwakil, FPGA realizations of high speed switching-type chaotic oscillators using compact VHDL codes. *Nonlinear Dyn.* **93**(2), 819–833 (2018)
4. V.H. Carbajal-Gomez, E. Tlelo-Cuautle, J.M. Muñoz-Pacheco, L.G. de la Fraga, C. Sanchez-Lopez, F.V. Fernandez-Fernandez, Optimization and CMOS design of chaotic oscillators robust to PVT variations: INVITED. *Integration* (2018). <https://doi.org/10.1016/j.vlsi.2018.10.010>
5. V. Carbajal-Gomez, E. Tlelo-Cuautle, C. Sanchez-Lopez, F. Fernandez-Fernandez, PVT-robust CMOS programmable chaotic oscillator: synchronization of two 7-scroll attractors. *Electronics* **7**(10), 252 (2018a)
6. A.S. Elwakil, M.P. Kennedy, Construction of classes of circuit-independent chaotic oscillators using passive-only nonlinear devices. *IEEE Trans. Circuits Syst.-I* **48**(3), 289–307 (2001)
7. A.S. Elwakil, S. Özoguz, A system and circuit for generating “multi-butterflies”. *Int. J. Bifurc. Chaos* **18**(03), 841–844 (2008)
8. A.S. Elwakil, S. Ozoguz, M.P. Kennedy, Creation of a complex butterfly attractor using a novel Lorenz-type system. *IEEE Trans. Circuits Syst.-I: Fundam. Theory Appl.* **49**(4), 527–530 (2002)
9. D.A. Hsieh, Chaos and nonlinear dynamics: application to financial markets. *J. Finance* **46**(5), 1839–1877 (1991)
10. <http://fpgasoftware.intel.com/?edition=lite> (Release date: September) (2018)
11. S.M. Ismail, L.A. Said, A.A. Rezk, A.G. Radwan, A.H. Madian, M.F. Abu-Elyazeed, A.M. Soliman, Generalized fractional logistic map encryption system based on FPGA. *Int. J. Electron. Commun.* **80**, 114–126 (2017)
12. G. Kaddoum, Wireless chaos-based communication systems: a comprehensive survey. *IEEE Access* **4**, 2621–2648 (2016)
13. L. Kocarev, S. Lian, *Chaos-Based Cryptography: Theory, Algorithms and Applications*, vol. 354 (Springer, Berlin, 2011)
14. F. Lau, C.K. Tse, *Chaos-Based Digital Communication Systems* (Springer, Berlin, 2003)
15. E.N. Lorenz, Deterministic nonperiodic flow. *J. Atmos. Sci.* **20**(2), 130–141 (1963)
16. I. Pan, S. Das, Evolving chaos: identifying new attractors of the generalised lorenz family. *Appl. Math. Model.* **57**, 391–405 (2018)
17. A. Pano-Azucena, E. Tlelo-Cuautle, G. Rodriguez-Gomez, L. de la Fraga, FPGA-based implementation of chaotic oscillators by applying the numerical method based on trigonometric polynomials. *AIP Adv.* **8**(7), 075217 (2018)
18. A. Radwan, A. Soliman, A. El-Sedeek, MOS realization of the modified lorenz chaotic system. *Chaos Solitons Fract.* **21**(3), 553–561 (2004)
19. A.G. Radwan, S.H. AbdElHaleem, S.K. Abd-El-Hafiz, Symmetric encryption algorithms using chaotic and non-chaotic generators: a review. *J. Adv. Res.* **7**(2), 193–208 (2016)
20. E. Schöll, *Nonlinear Spatio-temporal Dynamics and Chaos in Semiconductors*, vol. 10 (Cambridge University Press, Cambridge, 2001)
21. D. Shah, R. Charasiys, V. Vyawahare, K. Pichhode, M. Patil, FPGA implementation of fractional-order chaotic systems. *Int. J. Electron. Commun.* **78**, 245–257 (2017)
22. S.H. Strogatz, *Nonlinear Dynamics and Chaos with Applications to Physics, Biology, Chemistry, and Engineering* (Westview Press, Boulder, 2014)
23. M.F. Tolba, A.M. AbdelAty, N.S. Soliman, L.A. Said, A.H. Madian, A.T. Azar, A.G. Radwan, FPGA implementation of two fractional order chaotic systems. *Int. J. Electron. Commun.* **78**, 162–172 (2017)
24. H. Wang, H.F. Liang, Z.H. Miao, A new color image encryption scheme based on chaos synchronization of time-delay Lorenz system. *Adv. Manuf.* **4**(4), 348–354 (2016)
25. G.C. Wu, D. Baleanu, Z.X. Lin, Image encryption technique based on fractional chaotic time series. *J. Vib. Control* **22**(8), 2092–2099 (2016)
26. S. Yu, J. Lü, W.K. Tang, G. Chen, A general multiscroll Lorenz system family and its realization via digital signal processors. *Chaos: an interdisciplinary. J. Nonlinear Sci.* **16**(3), 033126 (2006)
27. M.A. Zidan, A.G. Radwan, K.N. Salama, Controllable V-shape multiscroll butterfly attractor: system and circuit implementation. *Int. J. Bifurc. Chaos* **22**(06), 1250143 (2012)

**Publisher's Note** Springer Nature remains neutral with regard to jurisdictional claims in published maps and institutional affiliations.

## Affiliations

**W. S. Sayed<sup>1</sup> · A. G. Radwan<sup>1,2</sup>  · M. Elnawawy<sup>3</sup> · H. Orabi<sup>3</sup> ·  
A. Sagahyroon<sup>3</sup> · F. Aloul<sup>3</sup> · A. S. Elwakil<sup>2,4,5</sup> · H. A. Fahmy<sup>6</sup> · A. El-Sedeek<sup>1</sup>**

✉ A. G. Radwan  
agradwan@ieee.org

W. S. Sayed  
wafaasayed@engl.cu.edu.eg

M. Elnawawy  
b00049112@alumni.aus.edu

H. Orabi  
horabi@aus.edu

A. Sagahyroon  
asagahyroon@aus.edu

F. Aloul  
faloul@aus.edu

A. S. Elwakil  
elwakil@ieee.org

H. A. Fahmy  
hfahmy@alumni.stanford.edu

A. El-Sedeek  
aeah7@yahoo.com

<sup>1</sup> Engineering Mathematics and Physics Department, Faculty of Engineering, Cairo University, Giza 12613, Egypt

<sup>2</sup> Nanoelectronics Integrated Systems Center, Nile University, Cairo 12588, Egypt

<sup>3</sup> Department of Computer Science and Engineering, American University of Sharjah, Sharjah, United Arab Emirates

<sup>4</sup> Department of Electrical and Computer Engineering, University of Sharjah, PO 27272 Sharjah, United Arab Emirates

<sup>5</sup> Department of Electrical and Computer Engineering, University of Calgary, Alberta, Canada

<sup>6</sup> Electronics and Communications Engineering Department, Faculty of Engineering, Cairo University, Giza 12613, Egypt